Computer Modeling in Engineering & Sciences

Tech Science Press

DOI: 10.32604/cmes.2021.014575

ARTICLE

Adaptive Extended Isogeometric Analysis for Steady-State Heat Transfer in Heterogeneous Media

Weihua Fang[1], Tiantang Yu[2,*] and Yin Yang[3]

[1]Nanjing Automation Institute of Water Conservancy and Hydrology, Ministry of Water Resources, Nanjing, 210012, China

[2]Department of Engineering Mechanics, Hohai University, Nanjing, 211100, China

[3]Lake Research Institute, Hydraulic Research Institute of Jiangsu Province, Nanjing, 210017, China

[*]Corresponding Author: Tiantang Yu. Email: tiantangyu@hhu.edu.cn.

Received: 10 October 2020 Accepted: 11 December 2020

ABSTRACT

Steady-state heat transfer problems in heterogeneous solid are simulated by developing an adaptive extended isogeometric analysis (XIGA) method based on locally refined non-uniforms rational B-splines (LR NURBS). In the XIGA, the LR NURBS, which have a simple local refinement algorithm and good description ability for complex geometries, are employed to represent the geometry and discretize the field variables; and some special enrichment functions are introduced into the approximation of temperature field, thus the computational mesh is independent of the material interfaces, which are described with the level set method. Similar to the approximation of temperature field, a temperature gradient recovery technique for heterogeneous media is proposed, and based on the Zienkiewicz–Zhu recovery technique a posteriori error estimator is defined to automatically identify the locally refined regions. The convergence and performance properties of the developed method are verified by using three numerical examples. The numerical results show that (1) The convergence speed of the adaptive local refinement is faster than that of the uniform global refinement; (2) The convergence rate of the high-order basis functions is faster than that of the low-order basis functions; and (3) The existing inclusions change the local distributions of the temperature, and the extreme values of the temperature gradients take place around the inclusion interfaces.

KEYWORDS

Heterogeneous media; steady-state heat transfer; adaptive XIGA; LR NURBS; heat dissipation

1 Introduction

Heat transfer in heterogeneous media widely exist in many fields. Numerical simulation is an efficient method for solving the common heat transfer problem, and heat transfer problem in heterogeneous media has been investigated with various numerical methods, such as meshless method [1], discrete element method [2], finite element method [3–6] and lattice Boltzmann method [7–9].

Most of the numerical methods used for the heat transfer are based on the finite element method (FEM). However, owing to the requirement of element edges to be lined up with the

discontinuity (e.g., crack, material interface, hole boundary), mesh generation of heterogeneous structure is very time-consuming. In order to overcome the issue, the extended FEM (XFEM) [10] was developed by introducing some special enrichment functions into the FEM approximation, thus the computational mesh is not related to the internal discontinuities. Yu et al. [11] solved steady and unsteady temperature fields in heterogeneous materials using the XFEM. Yvonnet et al. [12] proposed a simple and effective numerical procedure for simulating the Kapitza thermal resistance at an arbitrarily shaped interface using the XFEM combined with the level set method, and high accuracy and robustness can be obtained. Zuo et al. [13] obtained the thermal field in concrete with cooling pipe using the XFEM. Stapór [14] solved nonlinear transient problems with a phase change using the XFEM. The XFEM is a very effective numerical method for modeling the discontinuity, however, it has several drawbacks, for instance, discretization errors exist for complex-shaped structures; only C^0-continuity of shape function exists; and mesh generation is still required. In order to overcome the above-mentioned shortcomings, the extended isogeometric analysis (XIGA) [15] was introduced by taking the spline functions used in the computer-aided design (CAD) as the shape functions in the XFEM. The XIGA possesses some desirable features besides those in the XFEM, for example, arbitrarily complex structure can be exactly represented, the higher-order continuity of shape functions can be easily obtained, and the traditional mesh generation process is avoided. Due to such excellent characteristics, the XIGA has been applied to solve various discontinuities [16–23].

The adaptive technique can enhance the computational efficiency and the accuracy. Recently, the adaptive XIGA for modeling the discontinuity has received much attention. In order to locally refine, the researchers proposed some splines with local refinement ability, such as T-splines [24,25], Hierarchical B-splines [26], PHT-splines [27], Hierarchical NURBS [28], and LR B-splines [29,30]. Nguyen-Thanh et al. [31,32] presented an isogeometric analysis based on PHT-splines which facilitates adaptive refinement, and solved two-dimensional solids and thin shell. Later, they presented a multi-patch isogeometric large deformation thin shell formulation based on RTH splines, and developed a stress recovery technique to drive the adaptive h-refinement procedure [33]. Recently, we proposed the adaptive LR B-splines based XIGA and successfully simulated inclusions [34], holes [35], and cracks [36–38]. Yang et al. [39] developed an adaptive XIGA based on the PHT-splines for cracked thin plates and shells.

The existing studies reveal the efficiency of the adaptive XIGA in modeling discontinuous problems. Studies on modeling heat transfer problems in heterogeneous media using an adaptive XIGA have not be found in literature. The purpose of this study is to solve the steady-state heat transfer problems in heterogeneous media using an adaptive XIGA. We modeled the steady-state heat transfer problems using an adaptive LR B-splines based IGA [40], so this work is an extension of our previous work [40]. The methods based on LR B-splines possess the adaptable and diversified local refinement scheme, however, the LR B-splines can not exactly represent some complex geometries. LR NURBS [41] by combining NURBS with the LR B-spline theory can effectively overcome this issue. Hence, the adaptive LR NURBS based XIGA is adopted in this work. The LR NURBS basis functions are utilized for the structure discretization and the approximation of field variables. The smoothed temperature gradient field [42] is constructed, and according to the Zienkiewicz–Zhu recovery technique [43], a posteriori error estimator is evaluated to guide the local refinement. The main advantages of the proposed method include: (a) The geometry can be exactly described, i.e., without the discretization error; (b) The computational mesh is not related to the material interfaces, so mesh generation for heterogeneous media is very simple, and good shape elements can be obtained; (c) Only the required regions are automatically

and locally refined; (d) The accuracy and the computational cost can be concurrently taken into account; and (e) Fast convergence rate is achieved.

The organization of this article is as follows: The main equations for steady-state heat transfer in heterogeneous media are described in Section 2; Section 3 presents the adaptive LR NURBS based XIGA for steady-state heat transfer in heterogeneous media; Section 4 demonstrates the accuracy and the effectiveness of the proposed method; and some main concluding remarks are given in Section 5.

2 Problem Description

An isotropic heterogeneous media is considered. According to the theory of heat transfer, the temperature T in isotropic solid satisfies the following differential equations and boundary conditions:

$$\nabla \cdot (k \nabla T) + q_v = 0 \tag{1}$$

with

$$T = \overline{T} \quad \text{on } \Gamma_1 \tag{2a}$$

$$-kT_{,n} = q_n \quad \text{on } \Gamma_2 \tag{2b}$$

$$-kT_{,n} = h(T - T_w) \quad \text{on } \Gamma_3 \tag{2c}$$

$$T_1 = T_2, \quad k_1 T_{1,n} = k_2 T_{2,n} \qquad \text{on } \Gamma_4 \tag{2d}$$

where k, k_1 and k_2 denote the thermal conductivity parameter; q_v is the heat source; $\overline{T}$ and q_n are the prescribed temperature and heat flux density on the boundary, respectively; T_w is the ambient temperature, while h is the convective heat transfer coefficient; T_1 and T_2 are the temperatures of two materials on the interface; n denotes the outward normal on the boundary.

The first and the second class boundary conditions (Eqs. (2a) and (2b)) mean that the temperature function and the heat flux density on the boundary of the object are known, respectively. The third class boundary condition (Eq. (2c)) refers to the convective or radiative heat transfer on the boundary of the object. Assumed the perfect contact between two different solids, continuous temperature and heat flux exist on the interface, which is known as the fourth class boundary condition (Eq. (2d)).

Based on the variational principle, the steady-state heat transfer problem in heterogeneous media may be changed into solving the extreme-value problem of the following function:

$$\prod = \int_\Omega \left(\frac{1}{2} k \left((T_{,x})^2 + (T_{,y})^2 \right) - q_v T \right) \mathrm{d}\Omega + \int_{\Gamma_2} q_n T \, \mathrm{d}\Gamma + \int_{\Gamma_3} h \left(\frac{T^2}{2} - T \ T_w \right) \mathrm{d}\Gamma \tag{3}$$

3 Adaptive LR NURBS Based XIGA for Heat Transfer Problem

3.1 XIGA for Steady-State Heat Transfer in Heterogeneous Media

From Eq. (2), we can find that the temperature is continuous across the material interface, but the temperature gradients are discontinuous. According to the XFEM theory, the XIGA approximation for the temperature field can be written as [11]

$$T(x, y) = \sum_{i \in \boldsymbol{I}_1} R_i(\xi, \eta) \, T_i + \sum_{j \in \boldsymbol{I}_2} a_j R_j(\xi, \eta) \, \psi \tag{4}$$

with

$$\psi = \sum_{i \in \boldsymbol{I}_1} |\phi_i| \, R_i(\xi, \eta) - \left| \sum_{i \in \boldsymbol{I}_1} R_i(\xi, \eta) \, \phi_i \right| \tag{5}$$

where R_i and R_j denote the LR NURBS basis functions [41], which are defined with the local coordinates (ξ, η) in the parametric domain; T_i and a_j are the temperature and the enrichment variable at control point i and j, respectively; $\boldsymbol{I}_1$ and $\boldsymbol{I}_2$ are the set of control points in the discretized domain and the set of control points whose supports are intersected by the material interface, respectively; ψ is the enrichment function, and ϕ_i denotes the level set function value at the ith control point.

Combining Eq. (3) with Eq. (4) and applying variation rule lead to

$$\boldsymbol{K}\boldsymbol{T} = \boldsymbol{F} \tag{6}$$

where $\boldsymbol{T}$ is the global temperature vector. $\boldsymbol{K}$ and $\boldsymbol{F}$ are the global heat transfer matrix and temperature load vector, respectively. In addition, the element contributions to $\boldsymbol{K}$ and $\boldsymbol{F}$ are written as

$$\boldsymbol{k}_{ij} = \begin{bmatrix} \boldsymbol{k}_{ij}^{TT} & \boldsymbol{k}_{ij}^{Ta} \\ \boldsymbol{k}_{ij}^{aT} & \boldsymbol{k}_{ij}^{aa} \end{bmatrix} \tag{7}$$

$$\boldsymbol{f}_i = [f_i^T \quad f_i^a] \tag{8}$$

where

$$\boldsymbol{k}_{ij}^{rs} = \int_{\Omega_e} \left(\boldsymbol{B}_i^r\right)^T \boldsymbol{D} \boldsymbol{B}_j^s \, \mathrm{d}\Omega + \int_{\Gamma_3} \left(\boldsymbol{R}_i^r\right)^T h \boldsymbol{R}_j^s \, \mathrm{d}\Gamma \quad (r, s = T, a) \tag{9}$$

$$\boldsymbol{f}_i^r = \int_{\Omega_e} q_v \left(\boldsymbol{R}_i^r\right)^T \mathrm{d}\Omega - \int_{\Gamma_2} q_n \left(\boldsymbol{R}_i^r\right)^T \mathrm{d}\Gamma + \int_{\Gamma_3} h T_w \left(\boldsymbol{R}_i^r\right)^T \mathrm{d}\Gamma \quad (r = T, a) \tag{10}$$

with

$$\boldsymbol{D} = \begin{bmatrix} k & 0 \\ 0 & k \end{bmatrix} \tag{11}$$

$$\boldsymbol{B}_i^T = \begin{bmatrix} R_{i,x} \\ R_{i,y} \end{bmatrix}, \quad \boldsymbol{B}_i^a = \begin{bmatrix} R_{i,x} & (R_i\psi)_{,x} \\ R_{i,y} & (R_i\psi)_{,y} \end{bmatrix} \tag{12}$$

$$\boldsymbol{R}_i^T = [R_i], \quad \boldsymbol{R}_i^a = [R_i \quad R_i\psi] \tag{13}$$

For elements without any enriched control point, the numerical integration is conducted with $(p+1) \times (q+1)$ integral points, where p and q are the order of LR NURBS basis function in the ξ and η directions, respectively. For elements containing the material interface, the sub-triangle scheme [36] is used, and seven integration points are applied in each sub-triangle element.

Taking into account the first class boundary condition (Eq. (2a)), the temperatures and enrichment variables of control points are solved with Eq. (6). It is noted that the temperature

approximation presented in Eq. (4) can directly satisfy the fourth class boundary condition [11], thus the fourth class boundary condition in this method does not need special treatment.

3.2 Error Estimation

According to the Zienkiewicz and Zhu method [43], we can use the smoothed temperature gradients instead of the exact value to conduct the error estimation. The temperature gradients across the material interface are discontinuous, similar to the temperature approximation, the approximation of the smoothed temperature gradients can be expressed as

$$\boldsymbol{G}^s = \sum_{i \in \boldsymbol{I}_1} \boldsymbol{R}_i(\xi, \eta)\, \boldsymbol{G}_i^* + \sum_{j \in \boldsymbol{I}_2} \boldsymbol{R}_j(\xi, \eta) \left(H(\xi, \eta) - H\left(\xi_j, \eta_j\right)\right) \boldsymbol{a}_j^* \tag{14}$$

with

$$\boldsymbol{R}_i = \begin{bmatrix} R_i & 0 \\ 0 & R_i \end{bmatrix} \tag{15}$$

where H equals 1 on one side of a material interface and -1 on the other side, $\boldsymbol{G}_i^*$ and $\boldsymbol{a}_i^*$ are the smoothed temperature gradient vector and the corresponding enrichment variable vector at the control point i, respectively.

Eq. (14) is rewritten in a matrix form, i.e.,

$$\boldsymbol{G}^s = \boldsymbol{R}^* \boldsymbol{g}^* \tag{16}$$

Through a least square fit between the temperature gradients $\boldsymbol{G}^h$ obtained from the XIGA and the smoothed temperature gradients $\boldsymbol{G}^s$, the following equation can be obtained

$$\Psi(\boldsymbol{G}^*) = \int_\Omega \left(\boldsymbol{G}^s - \boldsymbol{G}^h\right)^T \left(\boldsymbol{G}^s - \boldsymbol{G}^h\right) \mathrm{d}\Omega \tag{17}$$

Minimizing Eq. (17) about the unknown variable vector $\boldsymbol{g}^*$ yields

$$\boldsymbol{A}\boldsymbol{G}^* = \boldsymbol{B} \tag{18}$$

where

$$\boldsymbol{A} = \int_{\Omega_e} \boldsymbol{R}^* (\boldsymbol{R}^*)^T \mathrm{d}\Omega \tag{19}$$

$$\boldsymbol{B} = \int_{\Omega_e} (\boldsymbol{R}^*)^T \boldsymbol{G}^h \mathrm{d}\Omega \tag{20}$$

The previous studies [40,44] show that the error in heat dissipation can effectively evaluate the accuracy of the numerical method for the heat transfer problems. According to the Zienkiewicz and Zhu error estimation [43], the posteriori error estimator is calculated with the smoothed temperature gradients instead of the exact value. For one element with area Ω_e, the L_2 error norm in the heat dissipation and the heat dissipation norm of the smoothed temperature gradient field are given by

$$\|e\|^2 = \int_{\Omega_e} \left(\boldsymbol{G}^s - \boldsymbol{G}\right)^T \boldsymbol{D} \left(\boldsymbol{G}^s - \boldsymbol{G}^s\right) \mathrm{d}\Omega \tag{21}$$

$$\|q\|^2 = \int_{\Omega_e} \left(\boldsymbol{G}^s\right)^T \boldsymbol{D}\boldsymbol{G}^s \, \mathrm{d}\Omega \tag{22}$$

The relative error for each element is evaluated with the following equation:

$$\theta = \frac{\|e\|}{\|q\|} \times 100\% \tag{23}$$

4 Numerical Results

Three numerical examples are analyzed to demonstrate the accuracy and the effectiveness of the present method. The first example, whose exact solution is available, is used to test the accuracy of the method. The second example considers a plate with one circular inclusion. The third example simulates a plate with four circular inclusions. The quadratic-order LR NURBS basis functions are used if not special specified in the following examples.

4.1 A Bi-Material Ring

Consider a bi-material ring with fixed temperatures on the inner and outer surfaces, as shown in Fig. 1a. $r_1 = 2\ m$, $r_2 = 4.2\ m$, $r_3 = 6\ m$, $T_1 = 0°\mathrm{C}$, and $T_3 = 20°\mathrm{C}$. The materials of the inner and outer rings are ordinary concrete and foamed concrete, and the thermal conductivity coefficients of the ordinary concrete and the foamed concrete are 10 KJ/(mh°C) and 0.377 KJ/(mh°C), respectively. Due to the symmetry, a quarter of the bi-material ring is taken into account for the analysis, and the adiabatic boundary condition is imposed on the symmetry faces, as shown in Fig. 1b.

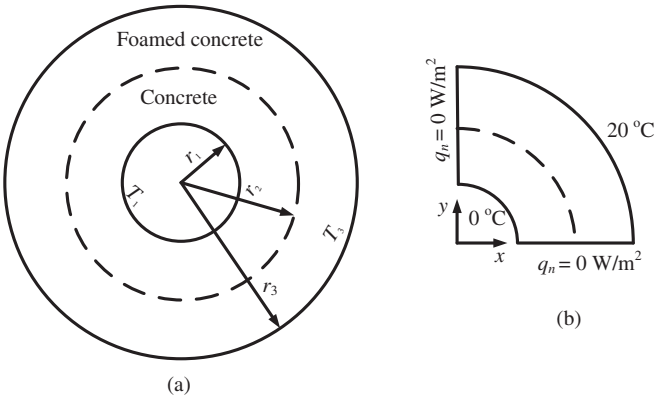

Figure 1: Problem definition for a bi-material ring

The exact temperatures in the bi-material ring are expressed as [45]:

$$T_2 = \frac{T_3 - T_1}{\frac{1}{2\pi k_1}\ln\frac{r_2}{r_1} + \frac{1}{2\pi k_2}\ln\frac{r_3}{r_2}} \quad (r = r_2) \tag{24a}$$

$$T = T_1 + \frac{T_2 - T_1}{\ln\frac{r_2}{r_1}}\ln\frac{r}{r_1} \quad (r_1 < r < r_2) \tag{24b}$$

$$T = T_2 + \frac{T_3 - T_2}{\ln \frac{r_3}{r_2}} \ln \frac{r}{r_2} \quad (r_2 < r < r_3) \tag{24c}$$

in which r is the radius.

Fig. 2 shows the uniform mesh and the corresponding control points labeled with circles for the original analysis. The orders of LR NURBS basis functions along the circumferential and radial directions are 2 and 1, respectively. It is noted that the computational mesh is independent of the material interface labeled in red line.

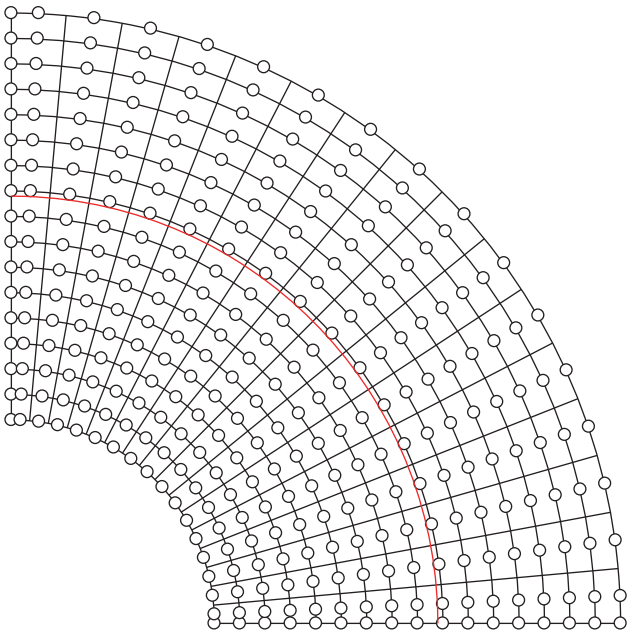

Figure 2: Original computational mesh and control points

Fig. 3 shows the four subsequent meshes in terms of the adaptive procedure. The local refinement first occurs around the material interface, then near the outer surface of the ring, finally around the inner surface of the ring and the material interface. These refined regions are as expected.

Figs. 4–6 show the distribution contours of the temperature and the temperature gradients obtained from the present method and the exact solution after four refinement steps, and the absolute errors are also plotted. From Figs. 4–6, it is found that the adaptive XIGA offers highly accurate results.

The temperatures along the radial direction are plotted in Fig. 7. The results obtained by the adaptive XIGA match well with the exact solution, which again verifies the excellent accuracy of the proposed method.

Fig. 8 presents the convergence curves of the L_2 error norm in the heat dissipation for both refinement schemes. It is obvious that the convergence speed of the adaptive local refinement (ALR) is faster than that of the uniform global refinement (UGR), and the same conclusion was obtain in the steady-state heat transfer problems in homogeneous media [40].

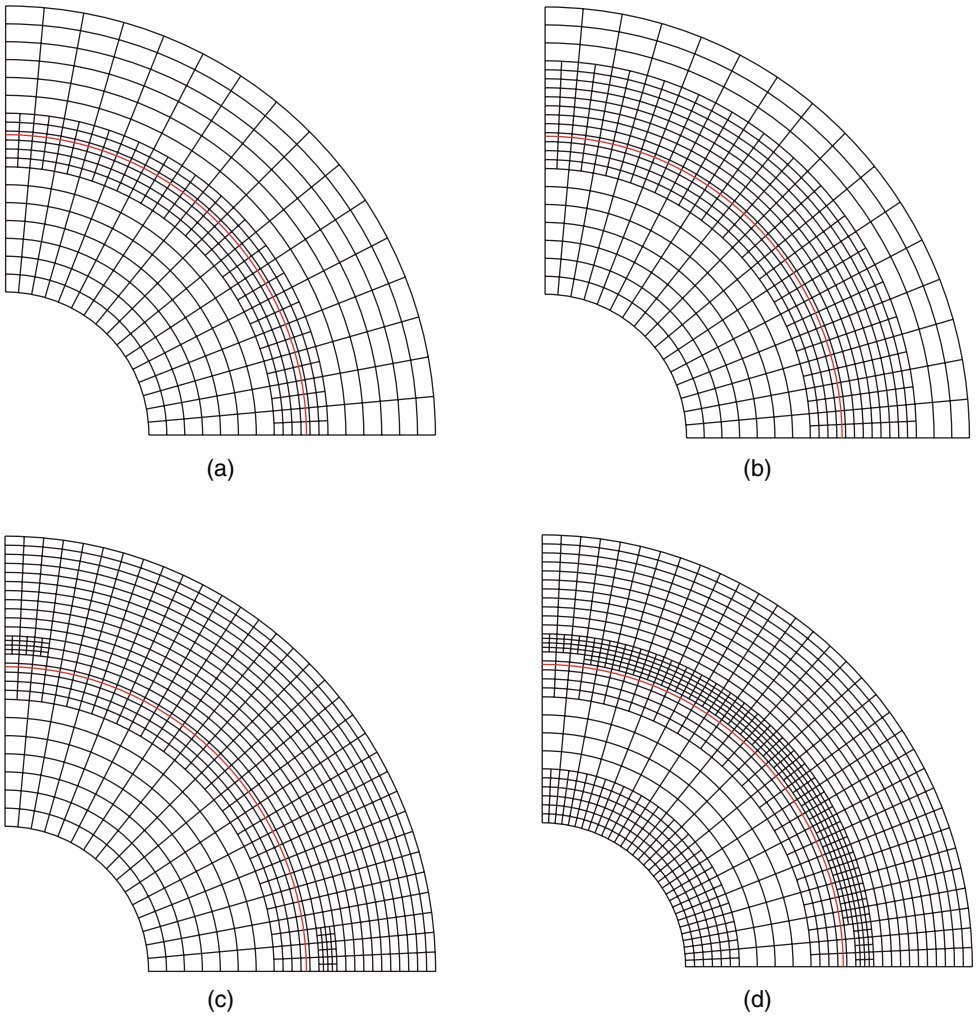

Figure 3: Locally refined meshes based on the error estimator at the Step 1(a), Step 2(b), Step 3(c) and Step 4(d)

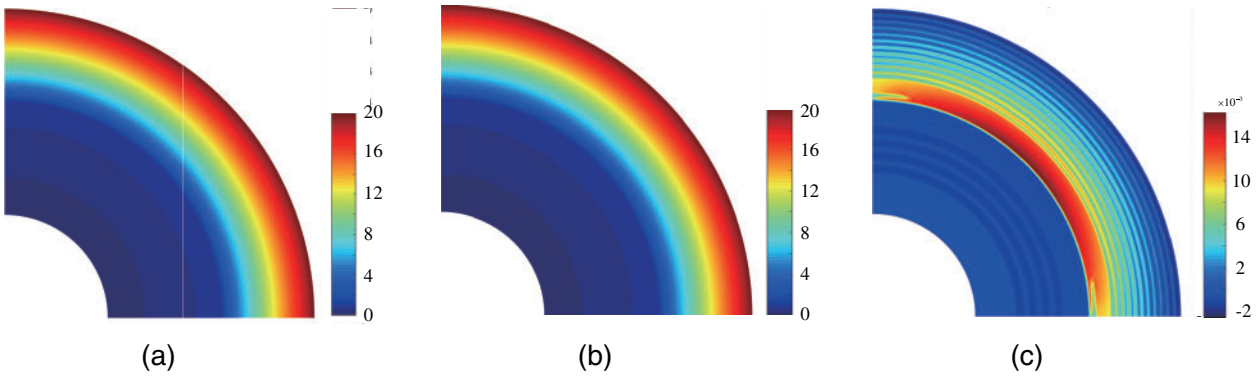

Figure 4: Temperature contours for the adaptive XIGA solution (a), the exact solution (b) and the absolute error (c)

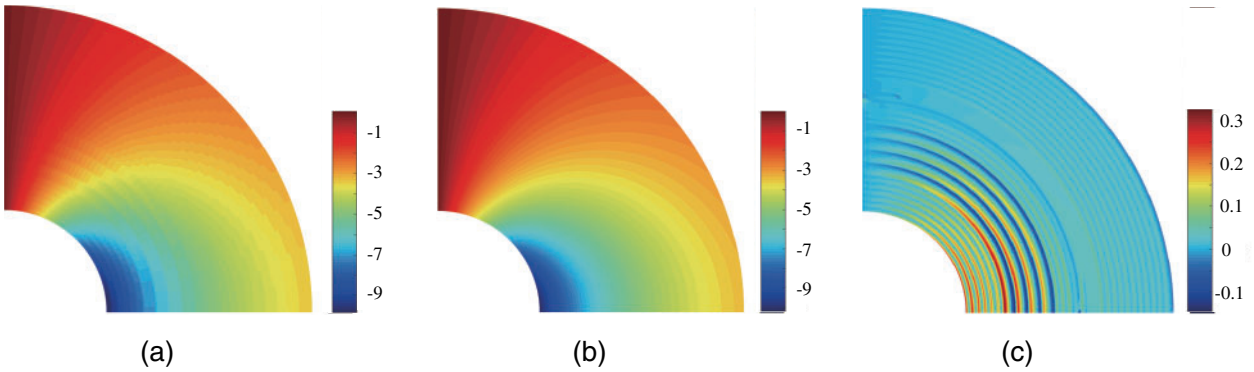

Figure 5: Temperature gradient contours in x-direction for the adaptive XIGA solution (a), the exact solution (b) and the absolute error (c)

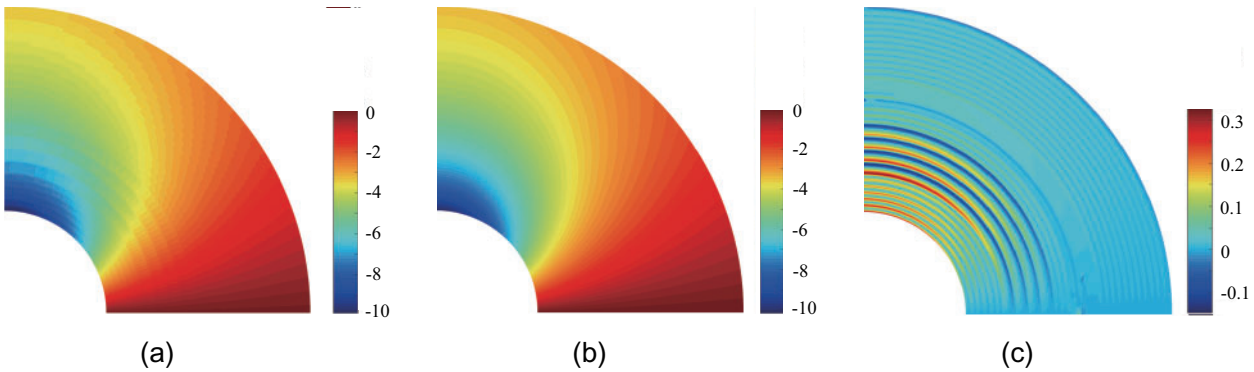

Figure 6: Temperature gradient contours in y-direction for the adaptive XIGA solution (a), the exact solution (b) and the absolute error (c)

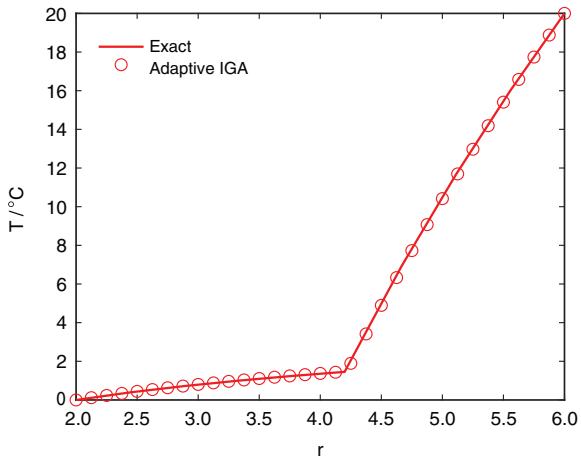

Figure 7: Temperatures along the radial direction

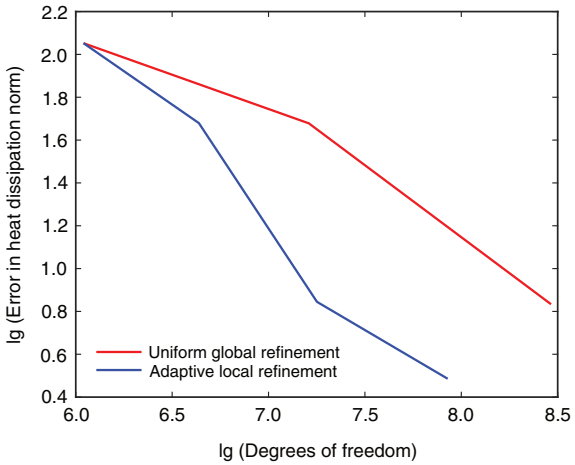

Figure 8: Comparison of convergence results between the ALR and the UGR

4.2 A Square Plate with One Circular Inclusion

The second example considers a square plate with one circular inclusion with a radius of 2 m, as shown in Fig. 9. The upper and lower surfaces are assumed to be adiabatic. Prescribed temperature on the left boundary is 400°C. The ambient temperature on the right side is 85°C, and the convective heat transfer coefficient equals 160 W/(m^2·°C). The thermal conductivity coefficients of materials B and A are 100 W/(m·°C) and 200 W/(m·°C), respectively.

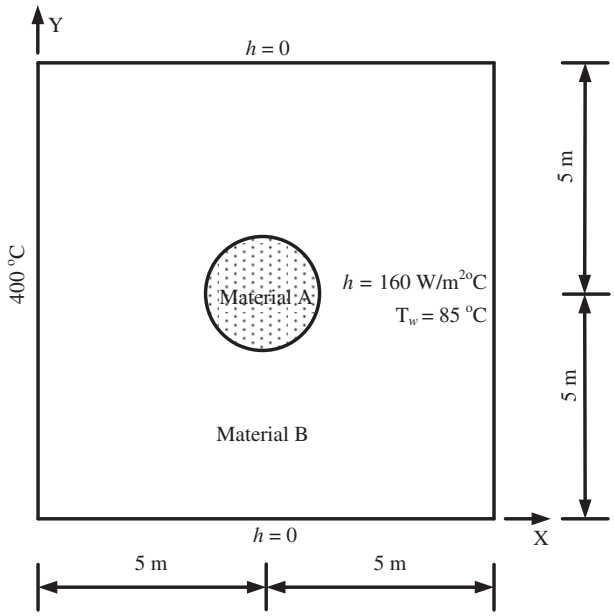

Figure 9: Problem definition for a square plate with one circular inclusion

Fig. 10 presents the initial mesh and the corresponding control points.

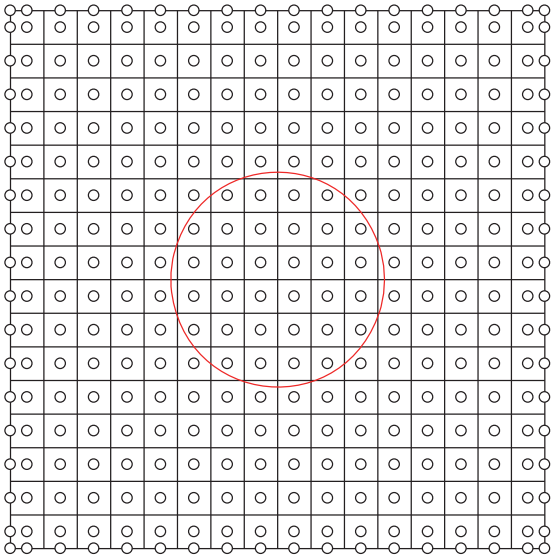

Figure 10: Original computational mesh and control points

Fig. 11 shows the three subsequent meshes in terms of the adaptive procedure. From Fig. 11, it is found that the local refinement takes place around the material interface, and the refined zone gradually approaches to the material interface with increasing the number of refinements. This shows that big error exits around the inclusion interface, as expected.

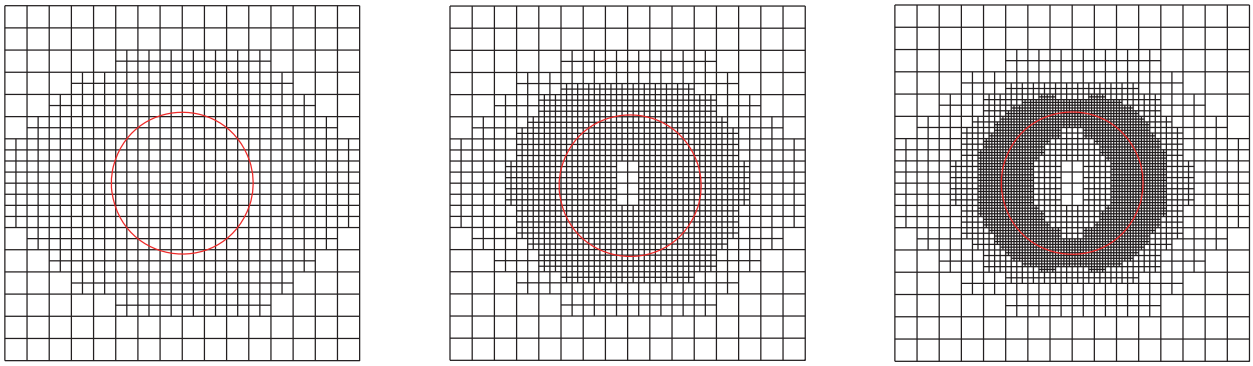

Figure 11: Locally refined meshes based on the error estimator at the Step 1(a), Step 2(b) and Step 3(c)

The distribution contours of the temperature and the temperature gradients in x and y directions after three refinement steps are shown in Figs. 12 and 13. The existing inclusion changes the local distribution of the temperature, and the extreme values of the temperature gradients take place around the inclusion interface.

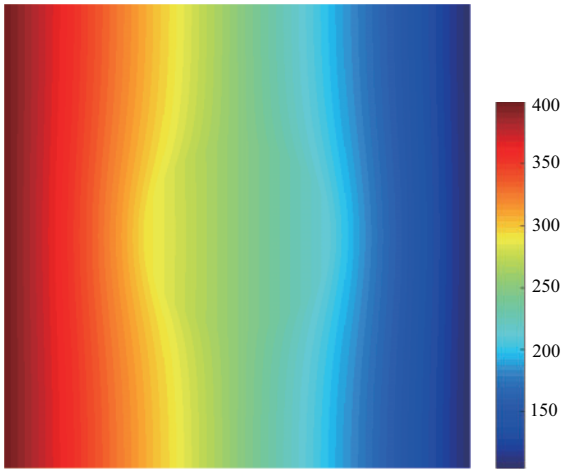

Figure 12: Temperature contours

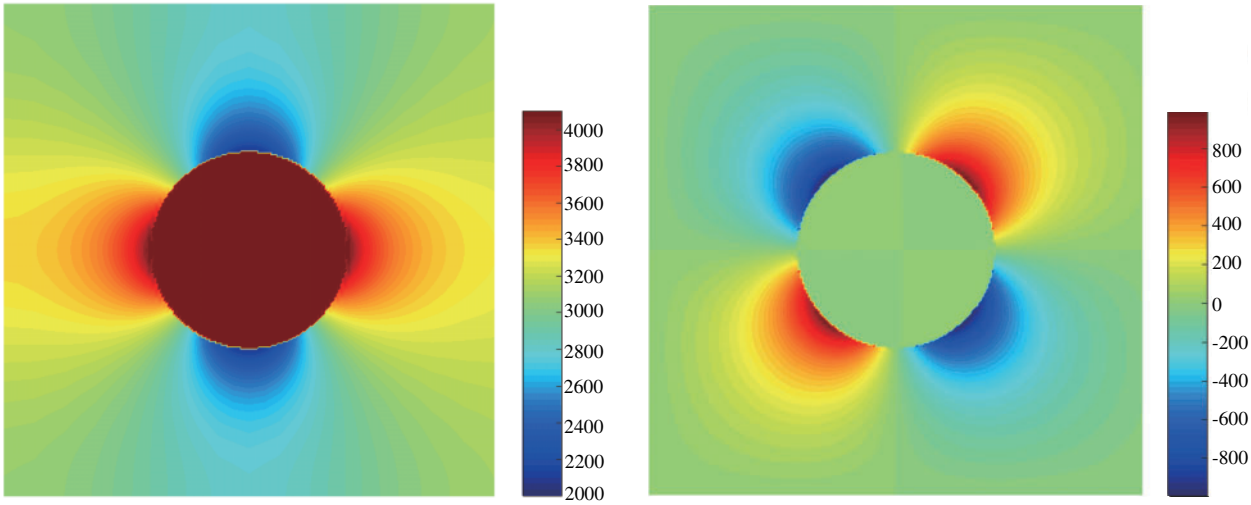

Figure 13: Temperature gradient contours in x-direction (a) and in y-direction (b)

Fig. 14 shows the variation of the relative error in heat dissipation norm with increasing the degrees of freedom (i.e., increasing the refinement step number) obtained with the adaptive XIGA with different basis orders. For $p = q = 1$, the present method becomes the standard extended finite element method. It is found that the convergence rate of the quadratic basis function is faster than that of the linear basis function with increasing the refinement step number.

4.3 A Square Plate with Four Circular Inclusions

In order to demonstrate the effectiveness of the present method for simulating the steady-state heat transfer in complex heterogeneous media, a square plate with four identical circular inclusions with a radius of 1.2m is taken into account, as shown in Fig. 15. The upper and lower boundaries are assumed to be adiabatic, and the prescribed temperatures on the left and right boundaries

are 400°C and 100°C, respectively. In addition, the thermal conductivity coefficient of matrix is 100 KJ/(mh°C), while the thermal conductivity coefficient of inclusions is 1000 KJ/(mh°C).

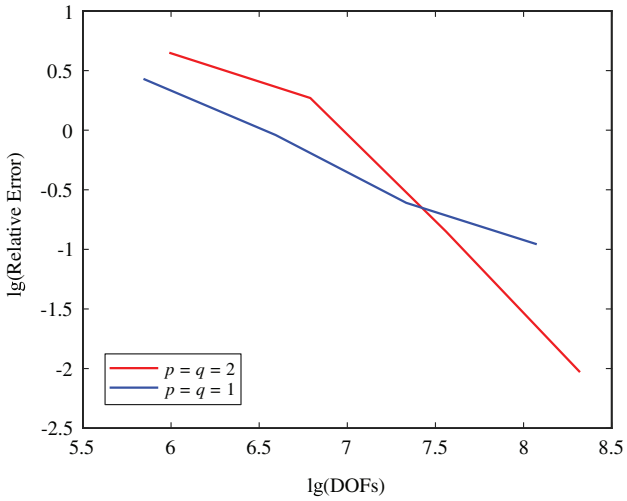

Figure 14: The variation of the relative error with the refinement step number

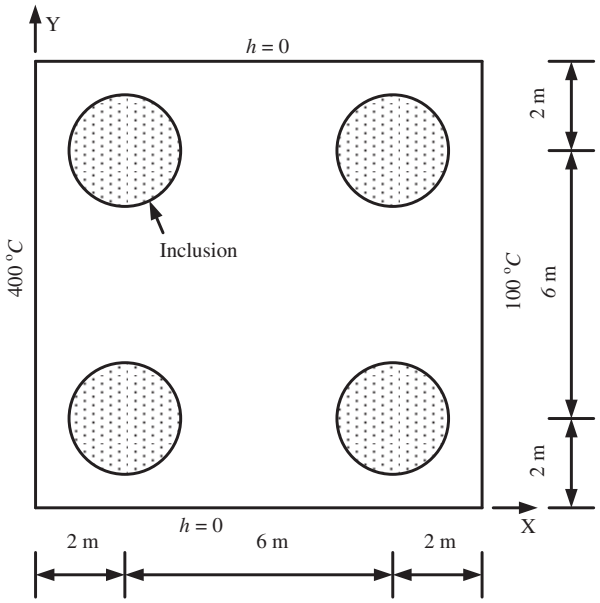

Figure 15: Problem definition for a square plate with four circular inclusions

The computation is first conducted on the uniform starting mesh, as shown in Fig. 16. The three subsequent meshes in Fig. 17 are generated according to the adaptive procedure. The refined regions are the same as those in the previous example, i.e., the local refinement takes place around the material interface, and the refined zone gradually approaches to the material interface with increasing the refinement steps.

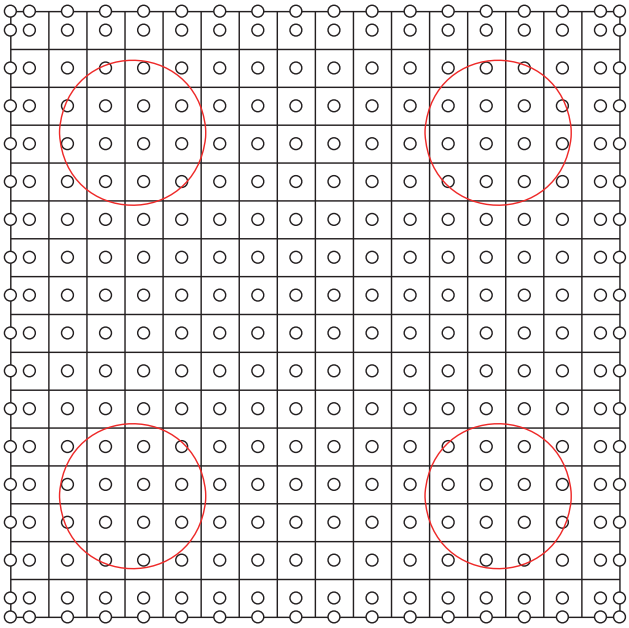

Figure 16: Original computational mesh and control points

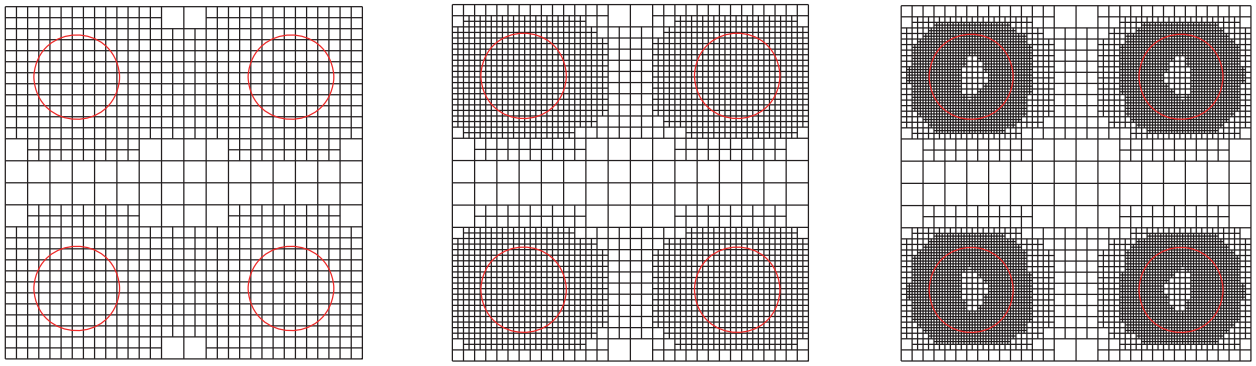

Figure 17: Locally refined meshes based on the error estimator at the Step 1(a), Step 2(b) and Step 3(c)

In addition, we plot the temperature contours in Fig. 18 and the temperature gradient contours in Fig. 19 on the final mesh. From Figs. 18 and 19, it is found that the existing inclusions change the local distributions of the temperature, the extreme values of the temperature gradients take place around the inclusion interfaces, and the distributions of the temperature gradients are almost the same around each inclusion.

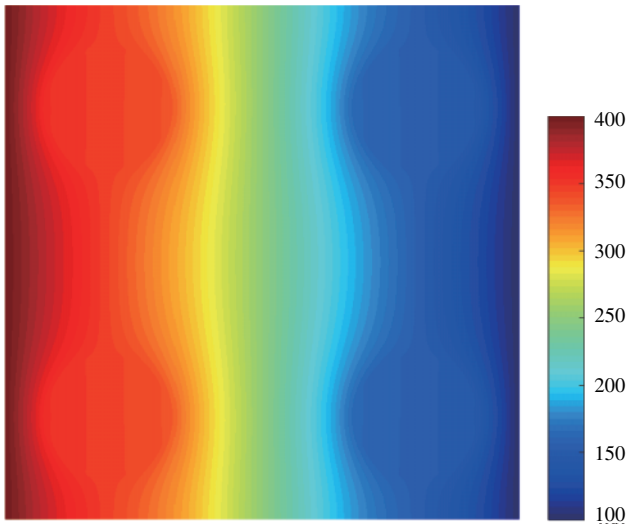

Figure 18: Temperature contours

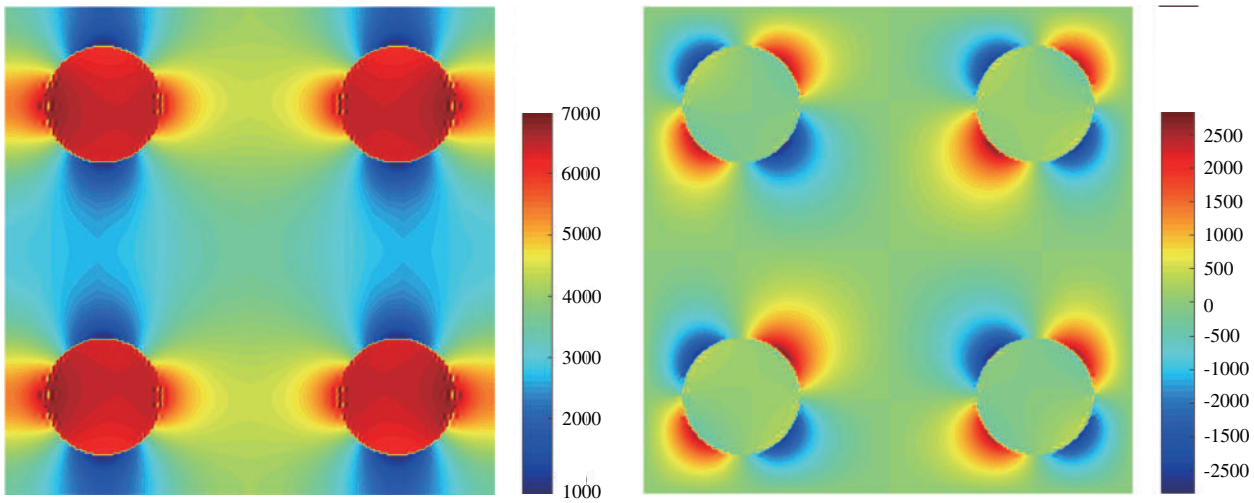

Figure 19: Temperature gradient contours in x-direction (a) and in y-direction (b)

5 Conclusions

An adaptive LR NURBS based XIGA for steady-state heat transfer problems in heterogeneous media is proposed. Because of the adaptable and diversified local refinement scheme and the exact description of complex geometry, the LR NURBS are adopted in the XIGA. The mesh is not related to the material interfaces by introducing special enrichment functions into the approximation of temperature field. A temperature gradient recovery technique for heterogeneous media is proposed, and the local refinement is automatically conducted based on the error estimator, which is constructed with the recovered temperature gradient field. Numerical results verify the excellent performance of the developed method.

The present approach owns some desirable features and its further developments include unsteady-state heat transfer and thermoelastic problems in heterogeneous media. In addition, the computation cost of the present method will be compared with that of conventional method by solving the large scale heterogeneous media.

Acknowledgement: The authors wish to express their appreciation to the reviewers for their helpful suggestions which greatly improved the presentation of this paper.

Funding Statement: The authors received no specific funding for this study.

Conflicts of Interest: The authors declare that they have no conflicts of interest to report regarding the present study.

References

1. Ahmadi, I., Aghdam, M. M. (2011). Heat transfer in composite materials using a new truly local meshless method. *International Journal of Numerical Methods for Heat & Fluid Flow, 21(3),* 293–309. DOI 10.1108/09615531111108477.
2. Haddad, H., Leclerc, W., Guessasma, M. (2018). Application of the discrete element method to study heat transfer by conduction in particulate composite materials. *Modelling and Simulation in Materials Science and Engineering, 26(8),* 85010. DOI 10.1088/1361-651X/aae63d.
3. Ramani, K., Vaidyanathan, A. (2016). Finite element analysis of effective thermal conductivity of filled polymeric composites. *Journal of Composite Materials, 29(13),* 1725–1740. DOI 10.1177/002199839502901304.
4. Deka, B., Dutta, J. (2020). Finite element methods for non-fourier thermal wave model of bio heat transfer with an interface. *Journal of Applied Mathematics and Computing, 62(1–2),* 701–724. DOI 10.1007/s12190-019-01304-8.
5. Lin, S., Smith, J., Liu, W. K., Wagner, G. J. (2017). An energetically consistent concurrent multiscale method for heterogeneous heat transfer and phase transition applications. *Computer Methods in Applied Mechanics and Engineering, 315,* 100–120. DOI 10.1016/j.cma.2016.10.037.
6. Vasilyeva, M., Stepanov, S., Spiridonov, D., Vasilév, V. (2020). Multiscale finite element method for heat transfer problem during artificial ground freezing. *Journal of Computational and Applied Mathematics, 371,* 112605. DOI 10.1016/j.cam.2019.112605.
7. Moudhaffar, N., Rihab, H., Sassi, B. N., Patrick, P. (2017). A three-dimensional enthalpic lattice Boltzmann formulation for convection-diffusion heat transfer problems in heterogeneous media. *Numerical Heat Transfer, Part A: Applications, 72(4),* 330–343. DOI 10.1080/10407782.2017.1372675.
8. Rihab, H., Moudhaffar, N., Sassi, B. N., Patrick, P. (2017). An enthalpy-based lattice Boltzmann formulation for unsteady convection-diffusion heat transfer problems in heterogeneous media. *Numerical Heat Transfer, Part A: Applications, 71(8),* 822–836. DOI 10.1080/10407782.2017.1309211.
9. Hosseini, S. A., Darabiha, N., Thévenin, D. (2019). Lattice Boltzmann advection-diffusion model for conjugate heat transfer in heterogeneous media. *International Journal of Heat and Mass Transfer, 132,* 906–919. DOI 10.1016/j.ijheatmasstransfer.2018.12.034.
10. Belytschko, T., Black, T. (1999). Elastic crack growth in finite elements with minimal remeshing. *International Journal for Numerical Methods in Engineering, 45(5),* 601–620. DOI 10.1002/(SICI)1097-0207(19990620)45:5<601::AID-NME598>3.0.CO;2-S.
11. Yu, T. T., Gong, Z. W. (2013). Numerical simulation of temperature field in heterogeneous material with the XFEM. *Archives of Civil and Mechanical Engineering, 13(2),* 199–208. DOI 10.1016/j.acme.2013.02.004.
12. Yvonnet, J., He, Q. C., Zhu, Q. Z., Shao, J. F. (2011). A general and efficient computational procedure for modelling the Kapitza thermal resistance based on XFEM. *Computational Materials Science, 50(4),* 1220–1224. DOI 10.1016/j.commatsci.2010.02.040.

13. Zuo, Z., Hu, Y., Li, Q. B., Liu, G. W. (2015). An extended finite element method for pipe-embedded plane thermal analysis. *Finite Elements in Analysis and Design, 102–103,* 52–64. DOI 10.1016/j.finel.2015.05.002.
14. Stapór P. (2015). The XFEM for nonlinear thermal and phase change problems. *International Journal of Numerical Methods for Heat & Fluid Flow, 25(2),* 400–421. DOI 10.1108/HFF-02-2014-0052.
15. De Luycker, E., Benson, D. J., Belytschko, T., Bazilevs, Y., Hsu, M. C. (2011). X-FEM in isogeometric analysis for linear fracture mechanics. *International Journal for Numerical Methods in Engineering, 87(6),* 541–565. DOI 10.1002/nme.3121.
16. Bui, Q. T. (2015). Extended isogeometric dynamic and static fracture analysis for cracks in piezoelectric materials using NURBS. *Computer Methods in Applied Mechanics and Engineering, 295,* 470–509. DOI 10.1016/j.cma.2015.07.005.
17. Ghorashi, S. S., Valizadeh, N., Mohammadi, S. (2012). Extended isogeometric analysis for simulation of stationary and propagating cracks. *International Journal for Numerical Methods in Engineering, 89(9),* 1069–1101. DOI 10.1002/nme.3277.
18. Nguyen-Thanh, N., Valizadeh, N., Nguyen, M. N., Nguyen-Xuan, H., Zhuang, X. et al. (2015). An extended isogeometric thin shell analysis based on Kirchhoff–Love theory. *Computer Methods in Applied Mechanics and Engineering, 284,* 265–291. DOI 10.1016/j.cma.2014.08.025.
19. Bhardwaj, G., Singh, I. V., Mishra, B. K. (2015). Stochastic fatigue crack growth simulation of interfacial crack in bi-layered FGMs using XIGA. *Computer Methods in Applied Mechanics and Engineering, 284,* 186–229. DOI 10.1016/j.cma.2014.08.015.
20. Singh, S. K., Singh, I. V., Mishra, B. K., Bhardwaj, G., Singh, S. K. (2018). Analysis of cracked plate using higher-order shear deformation theory: Asymptotic crack-tip fields and XIGA implementation. *Computer Methods in Applied Mechanics and Engineering, 336,* 594–639. DOI 10.1016/j.cma.2018.03.009.
21. Liu, S., Yu, T., Van Lich, L., Yin, S., Bui, T. Q. (2018). Size effect on cracked functional composite micro-plates by an XIGA-based effective approach. *Meccanica, 53(10),* 2637–2658. DOI 10.1007/s11012-018-0848-9.
22. Shojaee, S., Asgharzadeh, M., Haeri, A. (2014). Crack analysis in orthotropic media using combination of isogeometric analysis and extended finite element. *International Journal of Applied Mechanics, 6(6),* 1450068. DOI 10.1142/S1758825114500689.
23. Ghorashi, S., Valizadeh, N., Mohammadi, S., Rabczuk, T. (2015). T-spline based XIGA for fracture analysis of orthotropic media. *Computers & Structures, 147,* 138–146. DOI 10.1016/j.compstruc.2014.09.017.
24. Guo, M., Zhao, G., Wang, W., Du, X., Zhang, R. et al. (2020). T-splines for isogeometric analysis of two-dimensional nonlinear problems. *Computer Modeling in Engineering & Sciences, 123(2),* 821–843. DOI 10.32604/cmes.2020.09898.
25. Zhao, G., Yang, J., Wang, W., Zhang, Y., Du, X. et al. (2020). T-splines based isogeometric topology optimization with arbitrarily shaped design domains. *Computer Modeling in Engineering & Sciences, 123(3),* 1033–1059. DOI 10.32604/cmes.2020.09920.
26. Vuong, A. V., Giannelli, C., Jüttler, B., Simeon, B. (2011). A hierarchical approach to adaptive local refinement in isogeometric analysis. *Computer Methods in Applied Mechanics and Engineering, 200,* 3554–3567. DOI 10.1016/j.cma.2011.09.004.
27. Wang, J., Yang, Z., Jin, L., Deng, J., Chen, F. (2011). Parallel and adaptive surface reconstruction based on implicit PHT-splines. *Computer Aided Geometric Design, 28(8),* 463–474. DOI 10.1016/j.cagd.2011.06.004.
28. Wu, Z. J., Huang, Z. D., Liu, Q. H., Zuo, B. Q. (2015). A local solution approach for adaptive hierarchical refinement in isogeometric analysis. *Computer Methods in Applied Mechanics and Engineering, 283,* 1467–1492. DOI 10.1016/j.cma.2014.10.026.
29. Dokken, T., Lyche, T., Pettersen, K. F. (2013). Polynomial splines over locally refined box-partitions. *Computer Aided Geometric Design, 30(3),* 331–356. DOI 10.1016/j.cagd.2012.12.005.
30. Johannessen, K. A., Kvamsdal, T., Dokken, T. (2014). Isogeometric analysis using LR B-splines. *Computer Methods in Applied Mechanics and Engineering, 269,* 471–514. DOI 10.1016/j.cma.2013.09.014.
31. Nguyen-Thanh, N., Nguyen-Xuan, H., Bordas, S. P. A., Rabczuk, T. (2011). Isogeometric analysis using polynomial splines over hierarchical T-meshes for two-dimensional elastic solids. *Computer Methods in Applied Mechanics and Engineering, 200(21–22),* 1892–1908. DOI 10.1016/j.cma.2011.01.018.

32. Nguyen-Thanh, N., Kiendl, J., Nguyen-Xuan, H., Wuchner, R., Bletzinger, K. U. et al. (2011). Rotation free isogeometric thin shell analysis using pht-splines. *Computer Methods in Applied Mechanics and Engineering, 200,* 3410–3424. DOI 10.1016/j.cma.2011.08.014.
33. Nguyen-Thanh, N., Zhou, K., Zhuang, X., Areiase, P., Nguyen-Xuan, H. et al. (2017). Isogeometric analysis of large-deformation thin shells using RHT-splines for multiple-patch coupling. *Computer Methods in Applied Mechanics and Engineering, 316,* 1157–1178. DOI 10.1016/j.cma.2016.12.002.
34. Gu, J., Yu, T., Van Lich, L., Nguyen, T. T., Tanaka, S. et al. (2018). Multi-inclusions modeling by adaptive XIGA based on LR B-splines and multiple level sets. *Finite Elements in Analysis and Design, 148,* 48–66. DOI 10.1016/j.finel.2018.05.003.
35. Chen X., Gu J., Yu T., Qiu L., Bui T. Q. (2019). Numerical simulation of arbitrary holes in orthotropic media by an efficient computational method based on adaptive XIGA. *Composite Structures, 229,* 111387. DOI 10.1016/j.compstruct.2019.111387.
36. Gu, J., Yu, T., Lich, L. V., Tanaka, S., Yuan, H. et al. (2020). Crack growth adaptive XIGA simulation in isotropic and orthotropic materials. *Computer Methods in Applied Mechanics and Engineering, 365,* 113016. DOI 10.1016/j.cma.2020.113016.
37. Li, K., Yu, T., Bui, T. Q. (2020). Adaptive extended isogeometric upper-bound limit analysis of cracked structures. *Engineering Fracture Mechanics, 235,* 107131. DOI 10.1016/j.engfracmech.2020.107131.
38. Yu, T., Yuan, H., Gu, J., Tanaka, S., Bui, T. Q. (2020). Error-controlled adaptive LR B-plines XIGA for assessment of fracture parameters in through-cracked Mindlin-Reissner plates. *Engineering Fracture Mechanics, 229,* 106964. DOI 10.1016/j.engfracmech.2020.106964.
39. Yang, H. S., Dong, C. Y. (2019). Adaptive extended isogeometric analysis based on PHT-splines for thin cracked plates and shells with Kirchhoff–Love theory. *Applied Mathematical Modelling, 76,* 759–799. DOI 10.1016/j.apm.2019.07.002.
40. Yu, T., Chen, B., Natarajan, S., Bui, T. Q. (2020). A locally refined adaptive isogeometric analysis for steady-state heat conduction problems. *Engineering Analysis with Boundary Elements, 117,* 119–131. DOI 10.1016/j.enganabound.2020.05.005.
41. Zimmermann, C., Sauer, R. A. (2017). Adaptive local surface refinement based on LR NURBS and its application to contact. *Computational Mechanics, 60(6),* 1011–1031. DOI 10.1007/s00466-017-1455-7.
42. Huang, H. C., Lewis, R. W. (1989). Adaptive analysis for heat flow problems using error estimation techniques. *Sixth International Conference for Numerical Methods in Thermal Problems,* Swansea, UK.
43. Zienkiewicz, O. C., Zhu, J. Z. (1987). A simple error estimator and adaptive procedure for practical engineering analysis. *International Journal for Numerical Methods in Engineering, 24(2),* 337–357. DOI 10.1002/nme.1620240206.
44. Lewis, R. W., Huang, H. C., Usmani, A. S., Cross, J. T. (1991). Finite element analysis of heat transfer and flow problems using adaptive remeshing including application to solidification problems. *International Journal for Numerical Methods in Engineering, 32(4),* 761–781. DOI 10.1002/nme.1620320408.
45. Zhao, Z. N. (2008). *Heat transfer*. Higher Education Press, Beijing.